Journal of Power Sources 243 (2013) 110–117

Contents lists available at SciVerse ScienceDirect

Journal of Power Sources

journal homepage: www.elsevier.com/locate/jpowsour

Measurement of the internal cell temperature via impedance: Evaluation and application of a new method

Jan Philipp Schmidt [a,*], Stefan Arnold [a], André Loges [b], Daniel Werner [b], Thomas Wetzel [b], Ellen Ivers-Tiffée [a]

[a] Institut für Werkstoffe der Elektrotechnik, Karlsruhe Institute of Technology, Adenauerring 20b, 76131 Karlsruhe, Germany
[b] Institute of Thermal Process Engineering, Karlsruhe Institute of Technology, Karlsruhe, Germany

HIGHLIGHTS

- The internal temperature of a lithium-ion cell can be determined by EIS.
- If temperature gradients are present this temperature represents the mean value.
- SOC independence is obtained by selecting an appropriate measurement frequency.
- During operation the internal temperature exceeds the surface temperature by 20%.
- The application of this method can increase safety of battery operation.

ARTICLE INFO

Article history:
Received 19 March 2013
Received in revised form
29 May 2013
Accepted 3 June 2013
Available online 12 June 2013

Keywords:
Temperature
Lithium-ion
EIS
Measurement
Ohmic resistance
Impedance

ABSTRACT

Sensorless online temperature measurement of lithium-ion cells based on electrochemical impedance spectroscopy (EIS) measurements is introduced and applied to a commercial 2 Ah pouch cell. The method's sensitivity on temperature and state of charge (SOC) is investigated, taking a closer look to the selection of measurement frequency. The internal temperature is determined as precise as ±0.17 K with SOC status known and ±2.5 K with SOC status unknown at isothermal conditions.

Furthermore, the influence of a temperature gradient, as it will develop during cell operation, is studied in detail and the simulation results are validated experimentally. Finally, the method's ability to monitor the temperature is demonstrated during a thermal cool down.

1. Introduction

Large format Li-ion cells for automotive application are exposed to a broad temperature range from −40 °C to +70 °C, depending on operating conditions in combination with the thermal environment. At the same time, the behavior of Li-ion cells is strongly affected by temperature. At low temperatures the required performance may not be achieved or lithium metal plating may occur. This latter effect leads to a permanent loss of battery capacity and endangers battery safety by causing internal short circuits. At high temperatures, aging is accelerated, decreasing the life span significantly [1–3]. Even more elevated temperatures cause thermal runaway, as the exothermal decomposition of the solid electrolyte interface (SEI) was reported to start already at 100 °C [4,5] and 130 °C [6].

These few examples already show that cell temperature is one of the most important operating parameters. A comprehensive online detection of a change in cell temperature is essential to facilitate operation control regarding electrical performance, life span and security aspects. External sensors, i.e. thermocouples and resistance temperature detectors (RTDs), are well-established for temperature monitoring, but can hardly indicate the internal cell temperature. In addition, external temperature sensors cover only limited areas on the surface of the cell, hence hot spots may not be recognized. Furthermore, the thermal inertia of a cell, depending on cell size and design, may cause significant time delays between

* Corresponding author. Tel.: +49 721 608 47583.
E-mail address: jan.schmidt@kit.edu (J.P. Schmidt).

0378-7753/$ – see front matter © 2013 Elsevier B.V. All rights reserved.
http://dx.doi.org/10.1016/j.jpowsour.2013.06.013

the surface temperature signal and the temperature inside the cell. Even under steady-state conditions, the limited heat conductivity across the electrode stack and the volumetric heat source cause a considerable temperature difference between surface and cell core.

Different attempts to circumvent these problems and to quantify the deviation between core and surface temperature have been described in literature. Several authors estimated the core temperature using numerical models [7–9]. The accuracy of these simulations depends not only on the complexity of the underlying model but as well on the availability of material data and cell characteristics. Only few models are validated using internal temperature sensors, as experimental set-ups, even on the laboratory scale, are highly sophisticated [10].

Other authors proposed determining internal cell temperatures by electrochemical impedance spectroscopy [11]. This approach potentially facilitates the determination of the internal cell temperature without additional external sensors and corresponding wiring harness. A further potential advantage is the accuracy of the temperature measurement, as external temperature sensor data depends significantly on position, quality and reproducibility of the thermal contacts. A correlation between the phase angle of electrochemical impedance at a certain frequency and the internal temperature was suggested recently by Srinivasan et al. [11]. This method is based on the effect of SEI resistance changing with temperature, assuming isothermal cell behavior and independence of the impedance from the state of charge.

In this work the impedance is considered over a wide frequency band and the method presented in Ref. [11], is modified and further developed. The modified method is validated not only for cells with homogenous, but also for cells with inhomogeneous internal temperature distributions. Furthermore, the possibility of detecting the influence of local hot spots inside the electrode structure is discussed and the method is applied to determine the dynamic behavior of the internal cell temperature of pouch cells.

2. Measurement principle

The electrochemical impedance $Z = f(\mathrm{SOC}, T, f)$ of Li-ion cells is strongly depending on the temperature T, the state of charge SOC and the frequency f. Fig. 1 shows the logarithmic amplitude of the impedance of the investigated Li-ion cell plotted versus the frequency in a temperature range of −40 °C–40 °C. For these temperatures and a constant SOC of 50% the impedance amplitude changes over one to three decades for the depicted frequency range.

The dependence of the impedance on temperature is utilized in the presented method to determine the temperature using the inverse function $T = f^{-1}(Z, \mathrm{SOC}, f)$. To achieve a high variation of the impedance with temperature, a low frequency seems desirable at first sight. However, those low frequencies include the charge transfer process which is highly dependent on the SOC, as it is reported for various materials in literature [12,13]. Following the results of these investigations, the dependence of the impedance and correspondingly of the temperature on SOC can be neglected for a sufficiently high frequency range. More precisely, the evaluation frequency f_m needs to be chosen high enough, to ensure all SOC-dependent processes exhibit relaxation times well above $1/(2\pi f_m)$.

Fig. 2 shows that the magnitude of the impedance depends on frequency, temperature and SOC. The shaded areas depict the magnitude range for a variation of the SOC from 10% to 90% for a constant temperature. As the magnitudes for different temperatures overlap in the low frequency region, a distinct determination of the temperature, without additional knowledge of the SOC, is not possible. However, for frequencies above 20 Hz the three depicted temperatures can be separated even for unknown SOC.

To illustrate the dependence of the impedance at a distinct frequency on the underlying processes, a behavioral model has been fitted and its results are shown for the investigated cell at a SOC of 15% and a temperature of 40 °C in Fig. 3. The sum of all fitted impedance elements is compared to a measured impedance spectrum, indicating a good fit. While the arcs 1–3 are not strongly dependent on the SOC and could be attributed to the SEI (compare [14]), arc 4 is strongly dependent on the SOC. The characteristic frequency of the latter process lies in the range of seconds and can be attributed to the charge transfer [12]. At even lower frequencies, the diffusion of lithium in the particles can be described by a straight line with a 45° slope, also exhibiting a strong dependence on SOC.

Consequently, the ideal frequency range for temperature measurement is localized at the high frequency end of the impedance spectrum. Here, the measured frequency response is connected to the ohmic resistance R_0 (compare blue dot Fig. 3), representing the ionic conductivity of the electrolyte and the electron conductivity of the cell tabs and electrodes.

However, impedance measurements on commercial cells at very high frequencies always reflect an induction effect as well, mainly caused by current flow through tabs and wiring in the measurement setup. Generally this effect increases with decreasing internal resistance of the cell. Considering the inductance, the intersection point of the measured impedance spectrum with the real axis

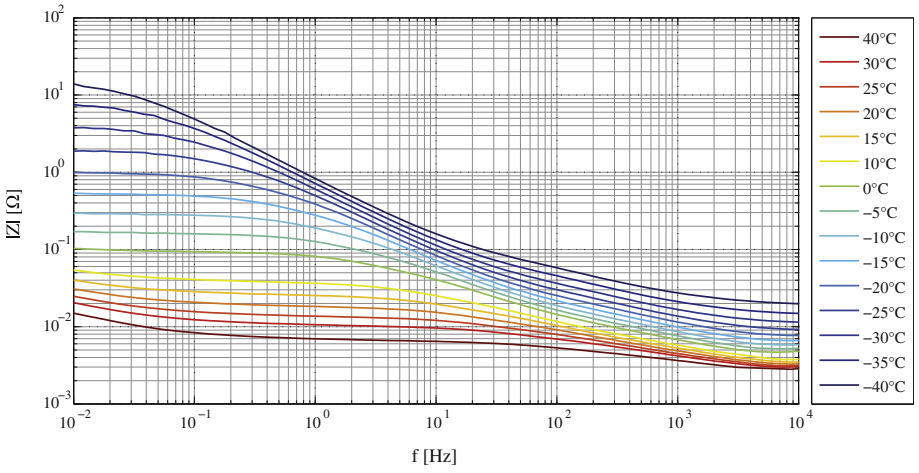

Fig. 1. Amplitude of the impedance of the investigated Li-ion battery cell at SOC = 50%.

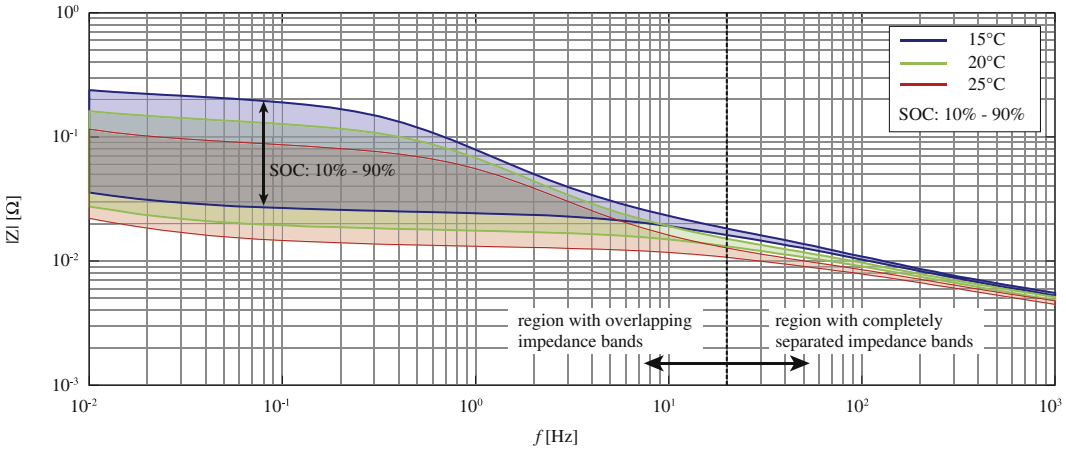

Fig. 2. Amplitude of the impedance of the investigated Li-ion battery cell at different SOC (10%–90%) and temperatures (15 °C, 20 °C, 25 °C).

(compare Fig. 3) cannot be interpreted as the actual ohmic resistance because it still contains information on other contributions, such as the one caused by the SEI [15]. As a good compromise a frequency of $f_m = 10.3$ kHz has been chosen, which shows only low inductive behavior and a slight dependence on the SOC. This remaining SOC-influence on the determination of the internal cell temperature will be discussed later.

Additionally, the inhomogeneous spatial temperature distribution under load effects the impedance based internal cell temperature determination, particularly for large cells. As the measurement represents an averaged internal cell temperature, the dependence on the temperature conditions been investigated thoroughly, using three basic validation cases:

- A: (spatially) homogeneous cell temperature
- B: (spatially) inhomogeneous cell temperature
- C: transient (and spatially inhomogeneous) cell temperature.

The experimental setup will be described in the next section, followed by a comprehensive discussion of the investigation results, including the validation of the proposed method.

3. Experiments

All experiments were carried out with a 2 Ah pouch cell (KOKAM, SLPB834374H), containing 57 stacked electrode layers. This Li-ion cell comprises a blend of $LiCoO_2$ and $LiNi_{0.8}Co_{0.15}Al_{0.05}O_2$ as cathode material and graphite as anode material. The

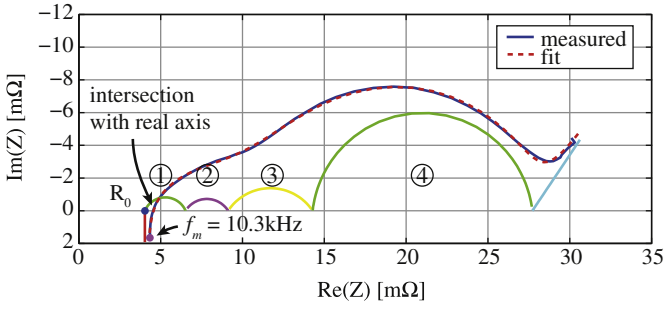

Fig. 3. Nyquist plot of impedance measurement (blue) at 23 °C and a SOC of 15% and the fitted behavioral model (red dotted line). Contributions of the single fitted equivalent circuit elements are plotted in different colors. The frequency $f_m = 10.3$ kHz for the temperature determination is marked as a magenta dot. (For interpretation of the references to color in this figure legend, the reader is referred to the web version of this article.)

electrochemical impedance measurements were carried out with a ZAHNER IM6 Workstation (ZAHNER-Elektrik GmbH & Co.KG, Germany), connected via electrical four terminal contact. The Li-ion cell was excited in pseudo-potentiostatic mode. For frequencies below 1 kHz an amplitude of 5 mV and for frequencies above an amplitude of 10 mV was chosen. The system linearity at both amplitudes was proven by the analysis of the higher harmonic components. The excitation frequency was varied within a range from 5 Hz to 150 kHz. All experiments were carried out inside a Weiss WK3-340/70 climate chamber (Weiss Umwelttechnik GmbH, Germany).

The chamber provides a defined thermal environment for the cell itself in case of the transient temperature distribution (case C) as described in detail below. For the experiments with homogeneous surface temperature (case A) and those with inhomogeneous thermal boundary conditions (case B), the cell surface temperature has been controlled using a sandwich-like structure, shown in Fig. 4. The pouch cell is thermally connected to aluminum heat transfer plates equipped with thermoelectric modules with a maximum heat power of 37 W. A designated temperature difference between the two lateral (*xy*-plane) surfaces of the battery cell can be imposed, while lateral temperature gradient inside the cell is avoided.

The temperature difference between both contact areas ($T_{surf,top} - T_{surf,bottom}$) is determined with calibrated thermocouples (type K), embedded in the aluminum plates and connected to a digital multimeter (Agilent 34970A). The temperature control (Cool Tronic) of the thermoelectric modules is realized by two PT1000 sensors, embedded within the aluminum plates. The remaining surfaces of the battery cell and the electric contacts are thermally insulated to maintain a perpendicular temperature gradient through the electrode stack.

3.1. Case A: homogeneous temperature distribution

At first, the electrochemical impedance was measured with a homogeneous temperature distribution. For that purpose, the climate chamber adjusted the temperature stepwise from 0 °C to 30 °C with increments of 5 K, while keeping the thermoelectric modules inactive. A period of 1 h was allowed for temperature equilibration of the Li-ion cell; after this period of time impedance measurements were performed.

In a first series, surface temperatures of 29.9, 24.9, 19.8, 14.7, 9.8, 4.9, and, 0.3 °C were measured at a central position on the upper lateral surface (see Fig. 3), at a constant state of charge of 50%. Those measurements are used later on as reference curve for the

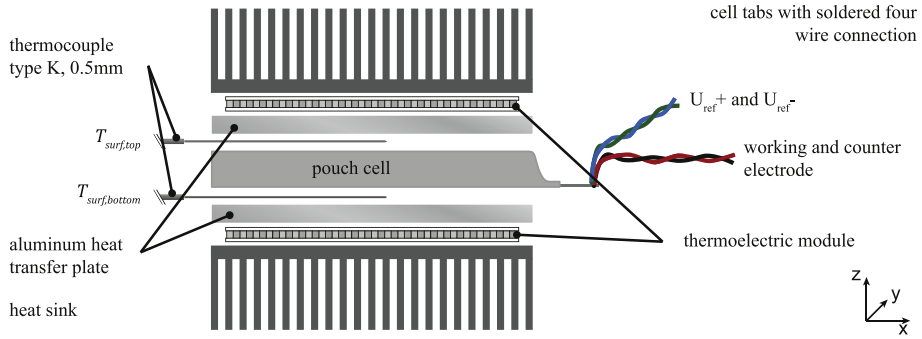

Fig. 4. Experimental set-up to apply a temperature gradient across the pouch cell via thermoelectric modules connected to an aluminum heat conduction plate. The cell is equipped with a four-wire contacting for impedance measurements, surface temperatures on top and bottom of the cell is measured with thermocouples type K.

correlation of the internal temperature with the measured $R(f_m)$. As during those measurements the cell was in thermal and electrochemical equilibrium, the surface temperature equals the internal temperature.

In a second series, the surface temperatures of 0.9, 5.0, 16.1, and, 24.3 °C were obtained under variation of the SOC from 10 to 90% with an increment of 20%. This facilitates the evaluation of the dependence between SOC and $R(f_m)$.

3.2. Case B: inhomogeneous temperature distribution

In this case a temperature difference between the two lateral surfaces (see Fig. 3) of the Li-ion cells was imposed. Table 1 shows the adjusted temperatures $T_{surf,top}$ and $T_{surf,bottom}$ during the first series of impedance measurements.

The maximum temperature difference was 16 K and both positive and negative temperature gradients between the two surfaces were applied to check the reproducibility. Consistency between the impedance measurements with inactive and with active thermoelectric modules was realized by performing measurements with similar temperatures on both thermoelectric modules. The climate chamber was set to 0 °C during all experiments to improve heat transfer from the thermoelectric modules.

In a second measurement series larger temperature differences up to 20 K were applied across the cell, while keeping $T_{surf,top}$ constant at 30 °C, see Table 2.

3.3. Case C: transient temperature distribution

In this case, the development of the internal temperature during a cool down process was investigated. During this experiment the bottom surface of the cell was thermally insulated and the temperatures were determined with type K thermocouples at three different positions: upper center surface $T_{surf,top}$, positive tab T_+ and negative tab T_- (see Fig. 5).

The chamber temperature T_{amb} was set to 0 °C and a zero-mean square-shaped current signal with an amplitude of 16 A was applied for internal thermal excitation of the cell. As the electrical resistance of the cell is comparably high at $T_{amb} = 0$ °C, the temperature rise inside the cell is distinct. After 1 h, the cell surface reaches the thermal steady state with a temperature of approximately 20 °C. Now, the thermal excitation was stopped and the electric impedance was measured at periodic intervals. The fastest temperature change can be observed immediately after the excitation shut-off. Thus, the sample rate was decreased with advancing thermal relaxation time from 2 Hz to 0.1 Hz, as denoted in Table 3. This facilitated a proper recording of the temperature response without overly increasing the dataset size.

To ensure constant properties of the Li-ion cell, a complete impedance spectrum was recorded before and after each measurement series in case C. The experiments showed that there was no drift in state of charge and no measurable change of the impedance behavior due to the continuous excitation signal.

Table 1
Case B: inhomogeneous temperature distribution. Temperatures $T_{surf,top}$ and $T_{surf,bottom}$ adjusted at perpendicular cell surfaces (see Fig. 3) during the first series of impedance measurements.

ΔT [K]	5	10	16	−5	−10	10	0	0	10	10	10	10
$T_{surf,top}$ [°C]	20	13	13	25	23	13	18	21	5	10	15	20
$T_{surf,bottom}$ [°C]	25	23	29	20	13	23	18	21	15	20	25	30

Table 2
Case B: inhomogeneous temperature distribution. Temperatures $T_{surf,top}$ and $T_{surf,bottom}$ adjusted at perpendicular cell surfaces (see Fig. 3) during the second series of impedance measurements.

ΔT [K]	20	16	12	8	4	0
$T_{surf\ top}$ [°C]	30	30	30	30	30	30
$T_{surf,bottom}$ [°C]	10	14	18	22	26	30

4. Results and discussion

4.1. Case A: homogeneous temperature distribution

The real part of $R(f_m)$ for $f_m = 10.3$ kHz, is plotted versus the inverse of the homogeneous temperature in Fig. 6. Furthermore, the dependence of $R(f_m)$ on the temperature was approximated with a conventional Arrhenius behavior of

$$R(f_m, T) = k \cdot e^{\frac{E_A}{RT}}, \quad (1)$$

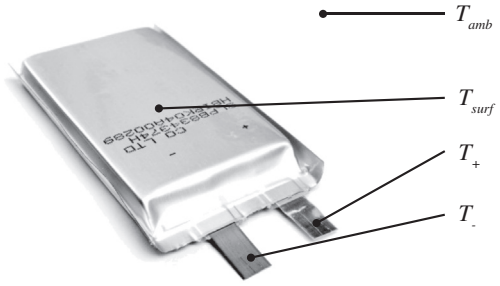

Fig. 5. Case C: transient temperature distribution: position of temperature measurements.

Table 3
Case C: transient temperature change. Sample rate with advancing thermal relaxation time.

Relaxation time	2 min	5 min	1 h
Sample rate	2 Hz	1 Hz	0.1 Hz

given in Fig. 6 as a green line. A systematic error between measurement and fit is observed. Considering the electric conductivity of the metallic collector as almost constant within the investigated temperature range, Equation (1) was modified by adding a constant resistance R_{col} for the collector:

$$R(f_m, T) = R_{col} + k \cdot e^{\frac{E_A}{RT}}. \quad (2)$$

Applying equation (2) to the measured data, the dependence of $R(f_m,T)$ is now in proper accordance (compare red line, Fig. 5), and the resulting activation energy E_A(arr + R) for the electrolyte conductivity is 0.26 eV. Another common approach to describe the temperature dependence of electrolyte conductivity is the Vogel–Tammann–Fulcher (VTF) equation, which describes the deviation from an ideal Arrhenius type equation [16]. Since the parameters are not interpreted physically and the extended Arrhenius approach already describes the measurement results accurately, the VTF equation has not been considered in this work.

However, not only the ohmic resistance R_0 and the closely related measured $R(f_m)$, but any other impedance measured at a constant frequency can be correlated with temperature as well. Srinivasan et al. [11] correlated the impedance measured at a frequency of 40 Hz. It is argued by these authors, that the phase angle solely depends on the temperature of the SEI. However, the activation energies presented in Ref. [11] show three distinct linear regions in a rather narrow temperature range. This leads to an increase of the activation energy for higher temperatures, reaching values between 0.4 eV and 0.8 eV. Usually such high values are attributed to the significant SOC dependent anodic and cathodic charge transfer process in Ref. [17]. The characteristic frequency and the contribution to the impedance at 40 Hz of the charge transfer process increase considerably with temperature. This may be an explanation for the varying activation energies found by Srinivasan et al. Therefore the internal temperature measurement should be considered to be dependent on SOC at this frequency.

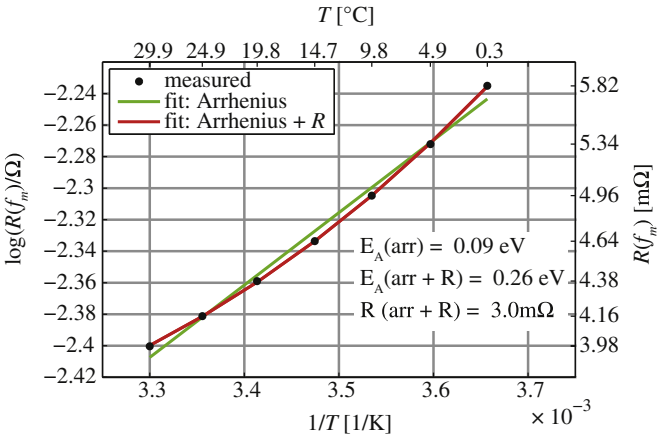

Fig. 6. Case A: homogeneous temperature distribution. $R(f_m)$, determined as the real part of the impedance at 10.3 kHz and a constant SOC of 50%, versus the inverse temperature. The fit to the Arrhenius Ansatz equation (1) is plotted as green line, the fit to the extended Arrhenius Ansatz equation (2) with an added ohmic resistance is plotted in red. (For interpretation of the references to color in this figure legend, the reader is referred to the web version of this article.)

In this study the applied frequency of 10.3 kHz is high enough to strongly limit the influence of the SOC on the measured ohmic resistance. This is quantified using an example shown in Fig. 7, where $R(f_m)$ is plotted versus the temperature for varying SOC. The black line depicts the Arrhenius fit according to Equation (2), already included in Fig. 5, at SOC of 50%. The arrows indicate the estimation error for the internal cell temperature, which would occur for a variation of the SOC at a temperature of 16.1 °C. Two factors determine the extent of the temperature deviation: The SOC-dependence of the impedance itself and the slope of the characteristic $R(f_m,T)$-curve. Steep gradients result in a minor temperature error. Therefore, a temperature value determined at low temperatures is more accurate, due to a nonlinear increase of $R(f_m)$ with decreasing temperature.

According to the results shown in Fig. 7, the temperature deviation ΔT is smaller than ±0.17 K if the SOC is known. A more accurate prediction of the internal cell temperature could be achieved by implementing more than one temperature dependent correlations of $R(f_m)$.

If the SOC is unknown, the consideration of a mean SOC (50% black line, Fig. 7) already results in a sufficient accurate temperature determination. The maximum error for $R(f_m)$ is still limited to 0.17 mΩ, resulting in a temperature deviation ΔT of ±2.5 K in the depicted temperature range from 0 °C to 25 °C.

In general it has to be taken into account that the accuracy of impedance measurement devices decreases for very low impedances and increasing frequencies. Therefore measurement accuracy decreases for (i) higher temperatures and (ii) decreasing internal resistance. As HEV/EV cells usually exhibit a very low impedance, the implementation of the necessary instrumentation in onboard applications is challenging and will have to be subject of future work.

4.2. Case B: inhomogeneous temperature distribution

According to Table 1, the measured values for $R(f_m)$ at inhomogeneous temperature distribution were plotted versus the mean value of temperatures $T_{surf,bottom}$ and $T_{surf,top}$ in Fig. 8. $R(f_m)$, again determined as the real part of the impedance at 10.3 kHz, coincides well with the parameterized Equation (2) (blue line) obtained from experiments with homogeneous temperature distribution. Therefore it can be concluded, that $R(f_m)$ determined at inhomogeneous temperature distributions reflect exactly the mean internal cell temperature in the investigated temperature range. The observed

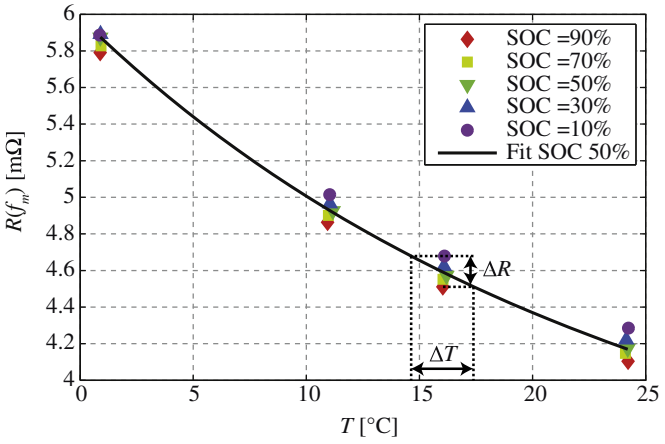

Fig. 7. SOC dependence of $R(f_m)$, determined as the real part of the impedance at 10.3 kHz. The fit to Equation (2) is shown as a black curve for SOC of 50%. The maximum temperature deviation ΔT arising from the dependence of $R(f_m)$ from SOC is illustrated by black dotted lines at a real cell temperature of 16 °C.

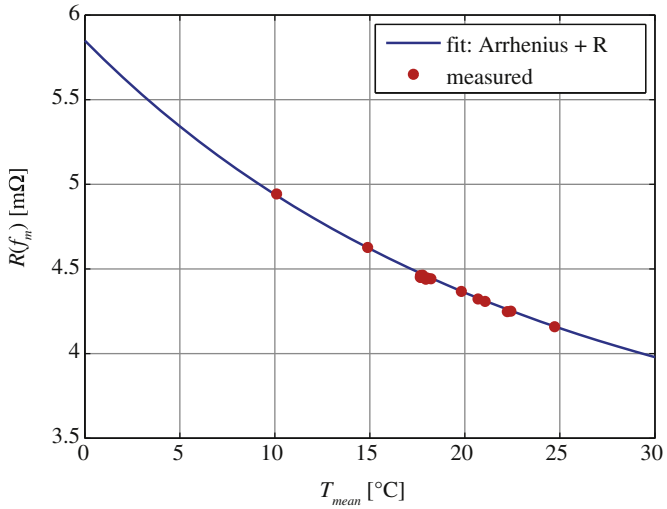

Fig. 8. Case B: Measured resistance $R(f_m)$ (red dots), versus the mean temperature of both surfaces. The straight blue line depicts parameterized Arrhenius behavior from case A. (For interpretation of the references to color in this figure legend, the reader is referred to the web version of this article.)

maximum deviation of $R(f_m)$ of 0.02 mΩ corresponds to an error in the determined internal cell temperature of 0.5 K.

However, the local temperature distribution inside the cell cannot be determined with the presented measurement method. Therefore the assumption of the algebraic mean value of bottom and top temperatures being a valid substitute for the mean cell temperature is investigated under varying internal temperature distributions. For this purpose, three different temperature distributions perpendicular to the electrodes have been considered based on different assumptions regarding the materials thermal conductivity inside the Li-ion cell:

- Constant: The temperature of the electrodes is constant along the *z*-axis (see Fig. 4) and equal to the mean temperature of top and bottom surface. This represents a situation where the cell housing has a very low thermal conductivity perpendicular to the surface compared to the electrode stack. In such condition, the complete temperature drop between top and bottom surface occurs in the (thermally insulating) cell housing. However, the thermal conductivity in *z*-direction in the cell stack is low, but is dominated by the high in-plane thermal conductivity of the collectors (copper and aluminum). This causes a homogenization of the cell core temperature via the welding points of the tabs.
- Linear: The temperature distribution is linear, which implies a constant temperature gradient. This corresponds to the assumption that the cell's thermal behavior can be described as a lump material with homogeneous thermal properties, while the homogenization by the high thermal conductivity of the collectors is neglected.
- Polynomial: The temperature along the *z*-axis is described with a polynomial of third order. In this scenario the thermal conductivity of housing and stack are assumed to be in the same order. This temperature distribution represents a combination of the aforementioned thermal characteristics in combination with a volumetric heat source under load.

The resulting temperature profiles perpendicular to the electrodes are given in Fig. 9 for the maximum temperature difference of 20 K along the *z*-axis. Since the pouch cell consists of a parallel connection of 56 single cells, the resulting resistance $R(f_m)$ can be

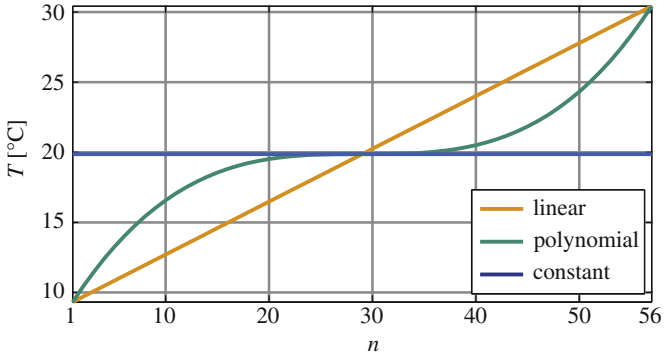

Fig. 9. Linear, polynomial and constant temperature profile across the electrodes of the pouch cell.

calculated as a parallel connection of resistances $R_n(f_m)$ of the individual cells according to the following equation:

$$R(f_m, T) = \left(\sum_{n=1}^{N} \frac{1}{R_n(f_m, T_n)} \right)^{-1}. \quad (3)$$

For the assumed temperature profiles (constant, linear or polynomial), the resistances $R_n(f_m,T_n)$ are determined using the parameterized Equation (2). All three profiles are depicted in Fig. 8 and the resulting overall resistances $R(f_m)$ are listed in Table 4. The resistances which would result from a homogenous cell temperature of 10 °C or 30 °C are given as the theoretical limits $R(f_m,T_{min})$ and $R(f_m,T_{max})$ in Table 4. The maximum deviation between all three temperature profiles is less than 1%, and the resistance value for the constant profile fits best with the measurement.

As previously described in the Experimental section, a second experiment has been performed with a constant temperature at the top surface and a temperature variation of the bottom surface of the cell. Results for lower temperature differences are shown in Fig. 10. The good fit of the resistance of an assumed constant temperature distribution and the measured value (see magnified inset in Fig. 10) suggest that electrode temperatures are almost constant in the measurements. However, it is important to note, that those differences are small and beyond measurement accuracy, thus making interpretations difficult. For a further investigation of the temperature distribution, the applied temperature difference might be increased even more. As the power capabilities of the used thermoelectric modules limit the temperature difference, this investigation could not be conducted yet.

However, since temperature differences (internal cell temperature to surface) in practical applications are below 20 K, it can be concluded that the exact temperature profile can be neglected and does not impede the monitoring of the internal temperature via impedance measurements.

Using the simple model Equation (3) not only the influence of a temperature profile arising from non-isothermal boundary conditions but also the influence of a hot spot can be simulated. This is demonstrated with the following scenario: a hot-spot is assumed to affect 2.5% of the electrode stack area, which is represented by one element of the sum of Equation (3). A temperature increase ΔT_{hot} in

Table 4
Resulting simulated overall ohmic resistance $R(f_m)$ for the different temperature profiles and for a constant maximum and minimum temperature. The measured value is given as $R(f_m,meas)$.

$R(f_m,T_{min})$	Constant	Polynomial	Linear	$R(f_m,T_{max})$	$R(f_m,meas)$
4.99 mΩ	4.366 mΩ	4.374 mΩ	4.385 mΩ	3.966 mΩ	4.3650 mΩ

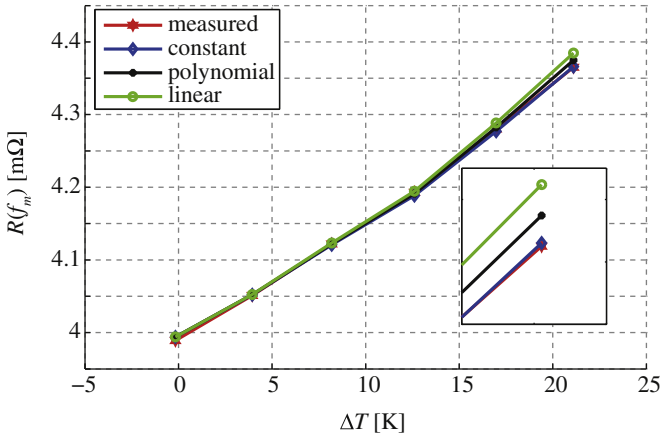

Fig. 10. Simulated and measured resistance $R(f_m)$ for a variation of the temperature difference of top and bottom cell surface ΔT.

one particular electrode with respect to the other electrodes is assumed and the resulting resistance value can be determined applying Equation (2). For a variation of ΔT_{hot} the resulting overall resistance can be calculated and is depicted in Fig. 11. The influence of a hot spot is visible, but the change of $R(f_m)$ for a hot spot with a temperature increase of 50 K alters the overall resistance $R(f_m)$ by only 1%. This sensitivity is well below the measurement accuracy in view of varying SOC and therefore not sufficient for an implementation in e.g. an EV's battery temperature control system.

4.3. Case C: transient temperature distribution

Impedance measurements are commonly performed in electrochemical equilibrium. However, measurements under load are also possible, allowing temperature monitoring in operation mode. For impedance measurements with a superposed load, signal to noise ratio of the sinusoidal measurement signal is decreased and therefore also the measurement quality of the impedance. Hence, we first concentrate on the influence of the temperature transient on $R(f_m)$ as proof of principle: internal temperature, determined as introduced above, is compared with external measurements during a cool down of a previously heated cell.

If only a single high frequency is measured, more than one impedance measurement per second can be performed, facilitating

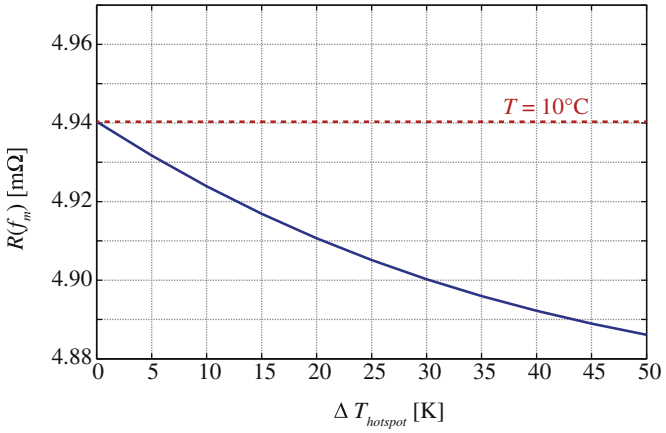

Fig. 11. Simulated resistance $R(f_m)$ of a pouch cell for a variation of the hot spot temperature increase (blue line) at an ambient temperature of 10 °C. The red line depicts the resistance $R(f_m)$ for an isothermal cell at 10 °C. (For interpretation of the references to color in this figure legend, the reader is referred to the web version of this article.)

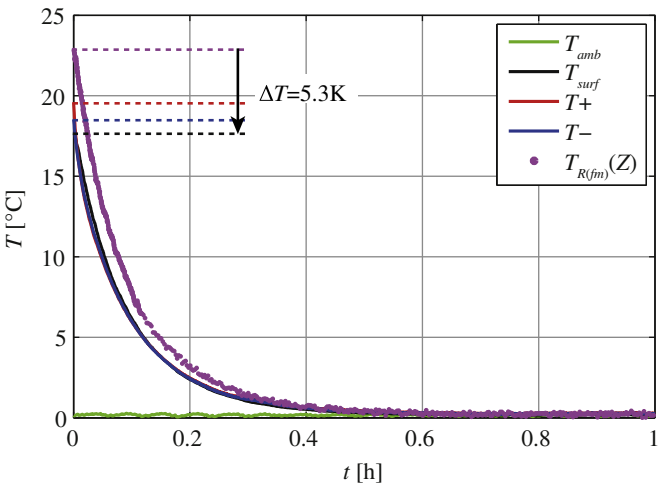

Fig. 12. Measured temperatures after switching off the current excitation for thermal relaxation of the cell in an ambient temperature of 0 °C, for the measurement positions of the different temperature signals refer to Fig. 4.

a continuous monitoring of the internal cell temperature. In the following, this method is demonstrated for the temperature response of a thermally excited pouch cell.

In order to heat the pouch cell, a zero-mean square-shaped current signal is applied. If this excitation is maintained for a certain period of time, a quasi-stationary state will be established, resulting in a constant temperature on the cell surface. The dissipated power during this quasi-stationary phase is calculated applying Equation (4) as 3.12 W.

$$P = \frac{1}{t_2 - t_1} \int_{t_1}^{t_2} (u(t) - U_{OCV}) \cdot i(t) \mathrm{d}t. \quad (4)$$

Directly after switching off the excitation signal, the impedance is repeatedly measured during the thermal relaxation phase. From these measured impedance data, the internal cell temperature is now determined and compared to the measured temperature from the temperature sensors versus time in Fig. 12. As can be observed, the measured values do not coincide directly after switching off the current excitation. The highest temperature of 22.9 °C is determined via impedance measurement for the mean internal cell temperature. The next lower temperature exhibits the positive tab with 19.3 °C. The negative tab is another 0.9 K below this temperature. The lowest temperature of 17.6 °C is measured at the top surface of the battery cell. The difference between the surface temperature of the cell and its internal temperature determined according to the above mentioned and validated method is 5.3 K. This corresponds to 23% of the temperature difference of cell surface to ambient temperature. This underlines the problems connected with using surface temperatures as representation of internal cell temperature, as already described in the Introduction.

At the same time, the potential of the newly developed method of impedance based internal cell temperature distribution is demonstrated. Further measurements of different transient processes, e.g. with transients in the thermal environment or combined electric load and thermal transients will have to be investigated to learn more about the characteristics and limits of the method.

5. Conclusion

Knowledge of the actual internal temperature is essential for operation control of Li-ion cells regarding electrical performance,

life span and security aspects. Sensorless temperature measurement via impedance spectroscopy was introduced as a promising on-line method to accurately determine the internal cell temperature.

The sensitivity depends on the selected measurement frequency: at low frequencies temperature and SOC dependence of the cell impedance is very distinct, but less pronounced at high frequencies. Therefore the application of high frequencies is beneficial, if the SOC is unknown. The internal temperature of a commercial 2 Ah pouch cell was determined as precise as $\pm$0.17 K with SOC status known and $\pm$2.5 K with SOC status unknown at isothermal conditions.

The proposed method yields the accurate mean internal cell temperature even during thermal transients. The results reveal that the internal cell temperature during such transients deviates significantly (in this experimental study more than 20%) from temperatures measured by external sensors located on the cell surface.

The presented method is a valuable alternative for temperature monitoring during cell operation and improves the accuracy in laboratory measurements.

As measurement accuracy decreases for (i) higher temperatures and (ii) decreasing internal resistance, implementation of the necessary instrumentation in HEV/EV onboard applications is challenging but has the potential of reduced instrumentation effort (external temperature sensors) and cost savings.

References

[1] M. Broussely, S. Herreyre, P. Biensan, P. Kasztejna, K. Nechev, R.J. Staniewicz, Journal of Power Sources 97–98 (2001) 13–21.
[2] M. Kassem, J. Bernard, R. Revel, S. Pélissier, F. Duclaud, C. Delacourt, Journal of Power Sources 208 (2012) 296–305.
[3] R.G. Jungst, G. Nagasubramanian, H.L. Case, B.Y. Liaw, A. Urbina, T.L. Paez, D.H. Doughty, Journal of Power Sources 119–121 (2003) 870–873.
[4] M.N. Richard, J.R. Dahn, Journal of the Electrochemical Society 146 (1999) 2068–2077.
[5] H. Maleki, G. Deng, A. Anani, J. Howard, Journal of the Electrochemical Society 146 (1999) 3224–3229.
[6] Z. Zhang, D. Fouchard, J.R. Rea, Journal of Power Sources 70 (1998) 16–20.
[7] S.C. Chen, Y.Y. Wang, C.C. Wan, Journal of the Electrochemical Society 153 (2006) A637–A648.
[8] S.C. Chen, C.C. Wan, Y.Y. Wang, Journal of Power Sources 140 (2005) 111–124.
[9] V. Srinivasan, C.Y. Wang, Journal of the Electrochemical Society 150 (2003) A98–A106.
[10] C. Forgez, D.V. Do, G. Friedrich, M. Morcrette, C. Delacourt, Journal of Power Sources 195 (2010) 2961–2968.
[11] R. Srinivasan, B.G. Carkhuff, M.H. Butler, A.C. Baisden, Electrochimica Acta 56 (2011) 6198–6204.
[12] D.P. Abraham, S. Kawauchi, D.W. Dees, Electrochimica Acta 53 (2008) 2121–2129.
[13] M.S. Wu, P.C.J. Chiang, J.C. Lin, Journal of the Electrochemical Society 152 (2005) A47–A52.
[14] M.D. Levi, G. Salitra, B. Markovsky, H. Teller, D. Aurbach, U. Heider, L. Heider, Journal of the Electrochemical Society 146 (1999) 1279–1289.
[15] S.S. Zhang, K. Xu, T.R. Jow, Electrochimica Acta 51 (2006) 1636–1640.
[16] M. Park, X. Zhang, M. Chung, G.B. Less, A.M. Sastry, Journal of Power Sources 195 (2010) 7904–7929.
[17] J. Illig, M. Ender, T. Chrobak, J.P. Schmidt, D. Klotz, E. Ivers-Tiffée, Journal of the Electrochemical Society 159 (2012) A952–A960.